Vol. 1(2), pp. 1-9, December 2022
DOI: 10.0001/AJPC2021.0207
ISSN 2021-xxxx

ASEAN Journal of Process Control

Research Article

Modeling and Simulation of Flat Plate Solar Collector Encompasses of Phase Change Material

Brandon Hua Yiik Yong[1], Norhuda Abdul Manaf[1]*, Minh Tri Luu[2], Ali Abbas[2]

[1] Department of Chemical and Environmental Engineering, Malaysia-Japan International Institute of Technology, Universiti Teknologi Malaysia, Kuala Lumpur, MALAYSIA.
[2] School of Chemical and Biomolecular Engineering, the University of Sydney, Sydney NSW, AUSTRALIA

*Corresponding Author: norhuda.kl@utm.my
Academic Editor: Jobrun Nandong
Received: 17 October 2022; Accepted: 14 November 2022; Published: 01 December 2022

Abstract: This paper studies the performance of flat plate solar collector (FPC) encapsulated with phase change material (PCM) using first principle mathematical model. PCM discretized equation based on latent heat and sensible heat were derived and implemented in MATLAB software for simulation. Different number of tubes (NT) of the PCM heat exchanger design and three types of PCMs with addition of different carbon material (paraffin, paraffin enhanced A, and paraffin enhanced B) were selected to evaluate the performance of PCM in FPC during charging and discharging processes. Heat transfer and efficiency of the FPC encapsulated with PCM are evaluated throughout these processes. Based on the simulation analysis, FPC design with 4 NT was the least efficient although it had the greatest heat transfer rate due to having higher heat transfer fluid (HTF) velocity which resulting in higher Reynolds numbers and heat transfer coefficient. FPC design with 12 NT which having efficiency of 0.84 and shorter PCM solidification time found to be the most promising design and beneficial in practice. Among three different PCMs, paraffin enhanced B with thermal conductivity of 3 W/m.K which having efficiency of 0.92 found to be the most promising PCM to be encapsulated with FPC. Besides, the discharging time of paraffin enhanced additive B was 3.8 times shorter than pure paraffin wax. The findings acquired from this study is valuable in identifying the practicality of integrated PCM with conventional FPC which utilize the PCM latent heat thermal energy storage (LHTES) as sustainable energy technology.

Keywords: Phase change materials, thermal energy storage, thermal conductivity, solar, flat plate solar collector, enhanced PCM

1. Introduction

Energy in Malaysia primary supplied from non-renewable crude oil, coal, and natural gas which will eventually depleted and lead to energy crisis in the future [1]. According to Malaysia Energy Statistics Handbook 2019, the total natural gas consumption in Malaysia was up to 18,852 Kilotons of Oil Equivalent (Ktoe) in 2018 [2]. Due to increasing non-renewable energy consumption which will lead to environmental issues, sustainable energy systems are getting much more attention [3].

There are many actions taken by government to mitigate the energy crisis problem such as development of renewable energy, hybrid technologies and other sustainable technologies. One of the most fundamental and most studied technologies for solar-powered water heating systems is flat plate solar collector (FPC) [4]. There are two main types of domestic water heating systems which are FPC and evacuated tube collector (ETC). FPC requires little maintenance and much cheaper than other type.

Besides, FPC able to collect both beam and diffuse radiation. However, most of the renewable energy encountered intermittency issues which indirectly decrease the performance of solar collector [5,6]. Besides, the gap between the energy demand and energy supply are large. Hence, approach such as incorporation of phase change materials (PCM) into commercial solar collector to store thermal energy has been introduced.

PCM latent heat thermal energy storage (LHTES) systems are attractive as it can store high capacity of thermal energy [7]. Basically, the operation mechanism of PCM is PCM will undergo melting process during the charging period and stores thermal energy as latent heat while PCM will solidify during discharging period and release the stored heat to heat up the water in contact. To improve the performance of commercial solar collector, PCM can be encapsulated into FPC which act as thermal energy storage. Consequently, thermal efficiency can be improved as the significant heat losses can be reduced when the FPC is at its highest temperature. Besides, space and costs can also be minimized as integration of PCM with FPC can eliminate the requirement of conventional storage tanks [8].

2. Methodology

Several assumptions were made before developing the mathematical model such as heat flow in angular direction is neglected, steady-state flow is considered, pressure drops in the copper tube where water flow is neglected, tube length is fixed at 1 m, mesh matrix of PCM node simulation is set at 10 x 40, the effect of natural convention is considered during charging and discharging cycle of PCM, thermal conductivity of paraffin enhanced additive A and additive B are assumed as 1 W/m.K and 3 W/m.K respectively and the direction of solar radiation is neglected in this study. After making assumptions, factors that affect the behavior of PCM such as PCM heat exchanger design configurations and thermal properties of PCM were identified and studied. The schematic of PCM model was draw using AutoCAD software to ease the progress in developing model as illustrated in Figure 1 which showing PCM shell-tube heat exchanger design with tubes arrangement.

Some formulation of PCM discretized equations based on first principles approach were derived before implemented into simulation tool. Energy balance for the PCM discretized equation shall be formed based on respective node. The energy balance for the respective node is shown in Equations 1-3. Equation 1 reflects interior PCM nodes while Equation 2 refers to top-middle PCM boundary node. Equation 3 refers to left-middle PCM boundary node.

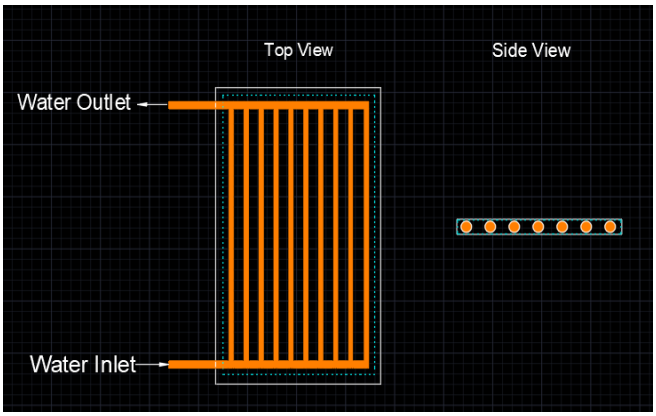

Figure 1 Schematic of PCM Model

$$\rho c_p \frac{\theta_p - \theta_p^o}{\Delta t} + \rho h_f \frac{f_p - f_p^o}{\Delta t} = \left(\frac{k_N r_N}{\Delta r^2 r_p}(\theta_N - \theta_p)\right) + \left(\frac{k_S r_S}{\Delta r^2 r_p}(\theta_S - \theta_p)\right) + \left(\frac{k_E}{\Delta x^2}(\theta_E - \theta_p)\right)\left(\frac{k_W}{\Delta x^2}(\theta_W - \theta_p)\right) \quad (1)$$

$$\rho c_p \frac{\theta_p - \theta_p^o}{\Delta t} + \rho h_f \frac{f_p - f_p^o}{\Delta t} = \left(\frac{2hr_i}{\Delta r(r_i + \frac{\Delta r}{4})}(\theta_{Water} - \theta_p)\right) + \left(\frac{2k_s r_S}{\Delta r^2 (r_i + \frac{\Delta r}{4})}(\theta_S - \theta_p)\right) + \left(\frac{k_E}{\Delta x^2}(\theta_E - T_p)\right) + \left(\frac{k_W}{\Delta x^2}(\theta_W - \theta_p)\right) \quad (2)$$

$$\rho c_p \frac{\theta_p - \theta_p^o}{\Delta t} + \rho h_f \frac{f_p - f_p^o}{\Delta t} = \left(\frac{k_N r_N}{\Delta r^2 r_p}(\theta_N - \theta_p)\right) + \left(\frac{k_S r_S}{\Delta r^2 r_p}(\theta_S - \theta_p)\right) + \left(\frac{2k_E}{\Delta x^2}(\theta_E - \theta_p)\right) \quad (3)$$

The mathematical model of PCM encapsulated with PCM is developed according to the discretized equations that basically based on the PCM latent heat and PCM sensible heat. MATLAB is selected as the simulation tool for the mathematical model in this case using available built-in "fsolve" function. In MATLAB, 2D geometry modelling was selected in this study and there were four heat flows which indicated the North node, N and South node, S (which in radial direction), East node, E and West node, W (which in axial direction). There are three different PCM nodes such as normal node, side boundary node and corner boundary node. Since the interface mechanism of those node types with surrounding nodes is different, for instance the shown corner only interfaces with two neighboring nodes, thus it is important to derive the energy balance for each node type. Energy balances are derived in simplest form as shown in Equation 4.

Accumulated heat=Heat enters from N+Heat enters from S+Heat enters from E+Heat enter from W (4)

The accumulated heat can take to form sensible and latent in mathematical form as shown in Equation 5 where the subscripts (N,S,E,W and P) represented positions of PCM nodes in North, South, West direction in which the "P" is known as central node (or current node), m represented mass of PCM in the 'P' node (kg), C_p represented heat capacity (J/kg.K), T represented Temperature (K), h_f represented heat of fusion (J/kg), f represented melt fraction in mass of the PCM stored in the "P" node, k represented thermal conductivity of PCM at particular position (W/m.K), Δr and Δs is the radial and axial distance for heat propagation between the nodes (m), and AP represented interfacial area between the 'P' node (m^2). The time domain was discretized using back-ward finite method. The rate of change in internal energy of a control volume (sensible heat and latent heat) is determined by the rate of heat receiving from the surrounding control volumes. Furthermore, the rate of heat transfer between the P node and the surrounding nodes can be determined by the temperature driving force. Throughout the derivations, the final equation was obtained as shown in Equation 6. The validation of the mathematical model was done by comparing the model prediction with the actual experimental data obtained from literatures [9-13]. This validated model is adapted based on the study conducted by Luu et al. [25]. The performance analysis of FPC encapsulated with different type of PCMs were conducted toward two parameters which are efficiency of FPC and heat transfer rate of PCMs.

$$m_p c_p \frac{dT_p}{dt} + m_p h_f \frac{df}{dt} = \left(\frac{k_N}{\Delta r} 2\pi r_N \Delta x (T_N - T_p)\right) + \left(\frac{k_S}{\Delta r} 2\pi r_S \Delta x (T_S - T_p)\right) + \left(\frac{k_E}{\Delta x} A_p (T_E - T_p)\right) + \left(\frac{k_W}{\Delta x} A_p (T_W - T_p)\right) \quad (5)$$

$$\theta_P \left(k_N r_N \frac{\Delta x}{\Delta r} + k_S r_S \frac{\Delta x}{\Delta r} + k_E r_p \frac{\Delta r}{\Delta x} + k_W r_p \frac{\Delta r}{\Delta x} + \rho c_p \frac{r_p \Delta x \Delta r}{\Delta t}\right) - k_N r_N \frac{\Delta x}{\Delta r}\theta_N - k_S r_S \frac{\Delta x}{\Delta r}\theta_S - k_E r_p \frac{\Delta r}{\Delta x}\theta_E - k_W r_p \frac{\Delta r}{\Delta x}\theta_W = r_p \frac{\Delta x \Delta r}{\Delta t}\rho c_p \theta_P^o + \rho h_f \frac{r_p \Delta x \Delta r}{\Delta t}(f_p^o - f_p) \quad (6)$$

3. Result and Discussion

In this study, the simulation was performed subjected to two different objectives which are different number of copper tubes (NT) and different type of PCMs. The simulation data was collected in MATLAB and relevant graphs were plotted to evaluate the performance of FPC encapsulated with PCMs in term of heat transfer rate of PCM and efficiency of FPC. The findings of this study are important in comparing the differences between the behavior of paraffin wax, paraffin enhanced additive A, and paraffin enhanced additive B with the purpose of selecting the most promising PCM to be encapsulated with FPC as latent thermal energy storage for better performance of FPC. Besides, this study also aims to find out how NT affect the performance of FPC in term of heat transfer rate and FPC efficiency.

3.1. Performance of FPC Encapsulated with Paraffin Subjected to Different Number of Tubes

Paraffin wax with thermal conductivity of 0.21 W/m.K [25] was used as the PCM that filled in the annulus of the simulation system. The dimension of module such as length, width and height are fixed at 2 m, 1 m, and 0.08 m respectively. The PCM filling areas and the heat transfer fluid (HTF) flow rates are varied according to different NT. In this study, water was the HTF that will flow inside the tube surrounded by PCM. PCM will absorb heat and begin to melt during charging cycle while PCM will release heat to warm the water inside the tubes during discharging cycle. Two conditions to finish the simulation which are simulation timed up after 24 hours of running time or PCM became completely solidified (f = 0) during discharging cycle. The phases of PCM can be determined by a subscript 'f' that written in MATLAB scripts. Subscript 'f' represented the melting fraction of PCM where 0 indicated the PCM was in solid phase whereas 1 indicated the PCM was in liquid phase.

Graph of heat transfer rate against time among different number of copper tubes (NT) was plotted and shown in Figure 2. According to Figure 2, PCM heat exchanger design with 4 NT found to have the greatest heat transfer rate, followed by design with 6 NT, 8NT, 12 NT and 16 NT. The design with 4 NT had the greatest heat transfer rate due to having the highest HTF velocity of 0.1151 m/s and HTF mass flow rate of 0.01175 kg/s. The HTF velocity for design with 4 NT, 6 NT, 8 NT, 12 NT and 16 NT were 0.1151 m/s, 0.0768 m/s, 0.0576 m/s, 0.0384 m/s and 0.0288 m/s respectively. The results proved that higher HTF velocity will lead to higher heat transfer rate as the heat extraction rate affected by water flow rate. Besides, higher HTF velocity increased the HTF mass flow rate which resulting in higher Reynolds numbers. Consequently, the heat transfer coefficient increased as the Reynolds numbers increased which resulting in greater heat transfer rate. Similar finding is also observed in [14].

Contrary design with 4 NT found to be the least efficient as the PCM stored the most heat energy but released the least stored heat energy to warm the water inside the tubes. Based on Figure 3, the efficiency of FPC design with 4 NT found to be 0.37, followed by 0.51, 0.64, 0.84, and 0.85 subjected to PCM heat exchanger designs with different NT. The efficiency of the system can be calculated using Equation 7. Efficiency is known as capability of system in discharging the stored latent heat to warm the water during discharging cycle. Hence, design with 4 NT was the least efficient as a result of the PCM absorbed 8993.57 kJ heat energy but only discharge up to 3371.68 kJ heat energy to warm the water. Similar finding can be observed in a study conducted by [15]. The thermal heat loss for FPC design with 4 NT was the highest which lead to low efficiency of FPC. Besides, as design with 4 NT had higher HTF flow rate and higher Reynold numbers compared to other NT, the heat energy utilization of the system will be decreased due to some expansion of heat exchanger zone [16].

$$\text{Efficiency} = (\text{Discharged Energy})/(\text{Charged Energy}) \quad (7)$$

Apart from having same inner tube outside radius (Ri) and inner tube inside radius (Rii), different FPC design have different value of outer tube inside radius (Ro). The outer tube inside radius (Ro) for design with 4 NT was 0.0798 m, followed by 0.0651 m, 0.0564 m, 0.0461 m, 0.0399 m. The design with 4 NT has the largest Ro which resulting in more PCM volume and PCM mass. Consequently, design with 4 NT have the greatest heat storage capacity. Similar finding is also observed in [17]. The study stated that higher flow rate will resulting in higher heat storing and releasing capacity.

Furthermore, design with 4 NT copper tubes have the largest Ro of 0.0798 m which resulting in smaller heat transfer area between the HTF and PCM. Smaller heat transfer area between HTF and PCM will cause slower heat exchange between the HTF and PCM through natural convention which resulting in longer solidification time of PCM during discharging cycle. Similar finding can also observe in study conducted by [18].

The simulation starts with charging cycle of PCM and ends with discharging cycle of PCM. The water and PCM enters at 25.0˚C before charging cycle commenced. The discharging cycle of PCM commences once the water temperature achieved the designated temperature which was 65.0˚C. Based on Figure 2, design with 12 NT managed to finish charging cycle and discharging cycle within the 24 hours simulation time. The PCM became completely solidified at 22.37 hour whereas PCM for design with 4 NT still undergo discharging cycle. For better understanding, 24 hours simulation time was equivalent with 2880 minutes in this study as the time step for collecting a PCM node data was fixed at 30 seconds. The PCM was not fully solidified during discharging cycle and remained partially liquid for

design with 4 NT. The result indicated that a portion of the heat energy stored by PCM during charging cycle was not able to discharge fully and became useless which resulting to low efficiency of FPC. Similar finding is also observed in [19].

In brief, PCM heat exchanger design with 12 NT had undergo complete charging and discharging cycle of PCM whereas design with 4 NT only undergo partial discharging cycle of PCM. A system integrated with PCM was considered efficient if the system able to utilize and discharge most of the stored latent heat to warm the water during discharging cycle of PCM. Although design with 16 NT had the highest efficiency of 0.85 but it is not ideal and costly compared to design with 12 NT. Hence, PCM heat exchanger design with 12 NT which having efficiency of 0.84 found to be the most promising design and beneficial in practice.

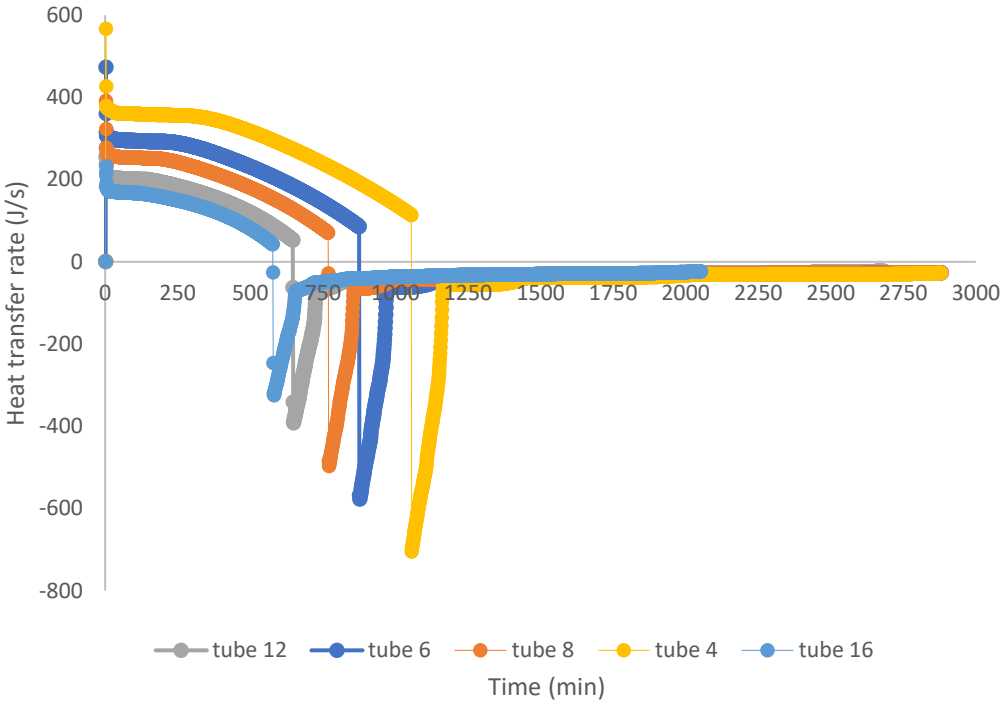

Figure 2 Heat transfer rate against time among different number of copper tubes

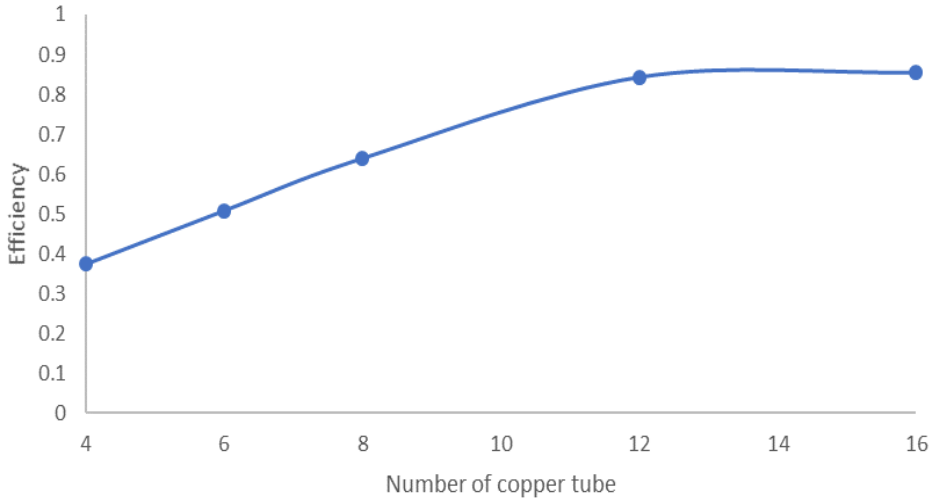

Figure 3 Efficiency of PCM for different number of copper tubes

3.2. Performance of FPC Encapsulated With Different Type of PCMs

Three hypothetical PCMs with addition of different carbon material (paraffin, paraffin enhanced additive A, and paraffin enhanced additive B) were used in this study and their thermal conductivity were 0.21 W/m.K, 1 W/m.K, and 3 W/m.K respectively. In this study, three simulations for three different PCMs were performed at same HTF flow rate which was 0.0384 m/s whereas FPC design with 12 NT was considered. Graph of heat transfer rate against time among different type of PCMs was plotted and

shown in Figure 3. According to Figure 4, paraffin enhanced additive B found to have the greatest heat transfer rate, followed by paraffin enhanced additive A and paraffin wax. Paraffin enhanced additive B has the greatest heat transfer rate compared to other PCMs due to having the highest thermal conductivity of 3 W/m.K. The results proved that higher thermal conductivity of PCM will lead to higher heat transfer rate. One of the limitations of utilize pure paraffin as LHTES was the low thermal conductivity of PCM, hence a lot of studies were conducted toward improving the thermal conductivity of pure PCM to enhance the overall performance of system integrated with PCM [20 - 23].

In this study, the addition of additives A and B into pure paraffin wax enriched the thermal conductivity of PCM. Consequently, higher thermal conductivity of PCM will increase the heat transfer coefficient which resulting in higher heat transfer rate of PCMs. Similar finding is observed in [12, 24]. The latent heat of enhanced PCMs decreased whereas the thermal diffusivity and thermal conductivity of enhanced PCMs increased after adding additives. Enhanced PCMs showed better performance in term of thermal conductivity and thermal stability. Enhanced PCMs had shorter heat releasing time as the heat transfer rate increased.

Heat transfer coefficient increased as heat thermal conductivity of PCM increased from 0.21 W/m.K to 3 W/m.K in this study which resulting in increment of Reynolds number. A higher heat transfer rate can be achieved with the increased heat transfer coefficient and Reynolds number. Similar finding is observed in [4, 25]. The heat transfer rate of PCM showed enhancement of 3.35 times after adding graphite to the pure PCM.

Shorter melting and solidification time during charging and discharging cycle of paraffin enhanced additive B can be observed in Figure 4. The result showed good agreement as paraffin enhanced additive B with higher thermal conductivity have higher heat transfer rate which resulting in faster heat exchange process between HTF and PCM. Similar finding is observed in [23]. Besides, as the heat transfer coefficient increased with the thermal conductivity increased, the thermal resistance of enhanced PCM will be decreased which resulting in greater surface heat flux. Hence, a better heat transfer rate of PCM can be obtained between the HTF and PCM with the increasing of thermal conductivity [26].

Graph of efficiency among different PCMs was plotted and shown in Figure 5. According to Figure 5, the efficiency of FPC with paraffin wax, paraffin enhanced additive A, paraffin enhanced additive B found to be 0.84, 0.89 and 0.92 respectively. The results indicated that PCM with higher thermal conductivity gave higher efficiency. According to Equation 7, the higher the capability of system in discharging the stored latent heat to warm the water during discharging cycle, the higher the efficiency of system can be attained.

The average charging storage for three PCMs was 2996.01 kJ. However, paraffin enhanced additive B provided an efficiency of 0.92 as it stored 2966.81 kJ of heat energy during charging cycle and released 2721.83 kJ of heat energy during discharging cycle. The thermal heat loss by the paraffin enhanced additive B was low which resulting in higher efficiency compared to other PCMs. Besides, majority of the heat energy stored by paraffin enhanced additive B during charging cycle was able to discharge almost fully to warm up the water inside tube.

According to Figure 4, paraffin enhanced additive B had shorter solidification time during discharging cycle of PCM, followed by paraffin enhanced additive A and paraffin wax. The results indicated that higher thermal conductivity of PCMs will gave shorter solidification time as the charging and discharging rate of enhanced PCM improved. Consequently, the overall efficiency of the system integrated with enhanced PCM showed better performance.

The total solidification time, heat storing and releasing time of paraffin enhanced additive B was shorter due to higher heat transfer rate and faster heat exchange between HTF and PCM with the help of natural convection within the system [27]. PCM with higher thermal conductivity will have shorter solidification time during discharging cycle of PCM as the thermal expansion and volume expansion due to phase change of PCM occurred during energy storage and regain process. The effect of natural convection within the system increased with the heat transfer rate which resulting in shorter charging and discharging cycle of PCM. The time for complete solidification for paraffin wax, paraffin enhanced additive A, and paraffin enhanced additive B was 22.37 hours, 11.34 hours, and 9.08 hours respectively.

As a result of high thermal conductivity and high transfer rate, the discharging time of paraffin enhanced additive B found to be 3.8 times shorter than pure paraffin wax. In brief, paraffin enhanced additive B with thermal conductivity of 3 W/m.K which having efficiency of 0.92 was the most promising PCM to be encapsulated with FPC to increase the performance of FPC.

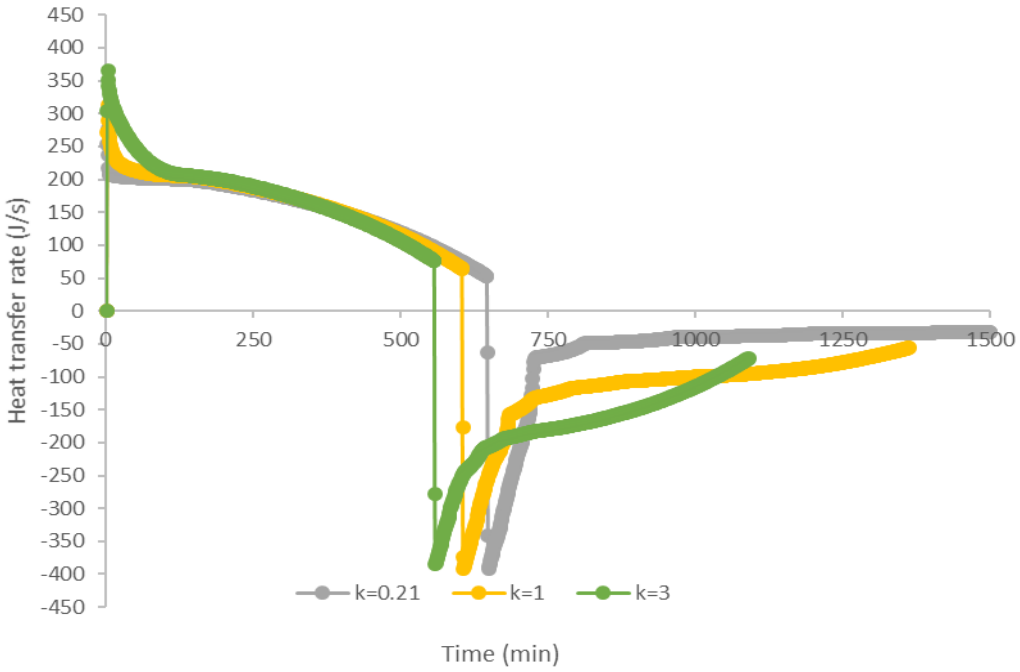

Figure 4 Heat transfer rate for different type of PCMs

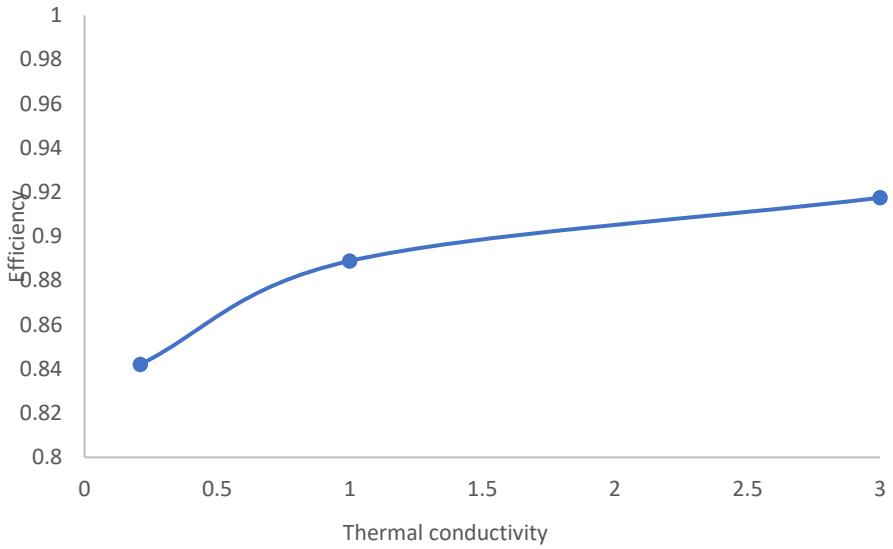

Figure 5 Efficiency for different types of PCMs

4. Conclusions

In this study, mathematical modelling of FPC encapsulated with PCM was simulated in MATLAB software by utilizing finite control volume approach. Based on the simulation analysis, PCM heat exchanger design with 4 number of tubes (NT) was the least efficient although it had the greatest heat transfer rate. Design with 4 NT found to have greatest heat transfer rate due to having higher heat transfer fluid (HTF) velocity. Higher HTF velocity increased the HTF mass flow rate which resulting in higher Reynolds numbers and higher the heat transfer coefficient. Consequently, greater heat transfer rate can be obtained. However, PCM heat exchanger design with 12 NT which having efficiency of 0.84 found to be the most promising design and beneficial in practice. The results stated that design with 12 NT showed shorter PCM solidification time and the PCM became completely solidified at 22.37 hour. When different thermal properties of PCMs were used in this study, paraffin enhanced additive B with thermal conductivity of 3 W/m.K which having efficiency of 0.92 found to be the most promising PCM to be encapsulated with FPC to increase the performance of FPC. Paraffin enhanced additive B provided an efficiency of 0.92 as it stored 2966.81 kJ of heat energy during charging cycle and released 2721.83 kJ

of heat energy during discharging cycle. The results indicated that the thermal heat loss by the paraffin enhanced additive B was low. Besides, the discharging time of paraffin enhanced additive B found to be 3.8 times shorter than pure paraffin wax as the heat transfer rate between PCM and HTF increased as the thermal conductivity increased. The times for complete solidification for paraffin wax, paraffin enhanced additive A, and paraffin enhanced additive B were 22.37 hours, 11.34 hours, and 9.08 hours respectively.

Acknowledgement
The authors wish to acknowledge financial support from Ministry of Education (MOE) through Malaysian Research University Network Young Researchers Grant Scheme, project no. R.K130000.7843.4L909 and R.K130000.7843.4L901.

References

1. Abd. Aziz, P. D., Wahid, S. S. A., Arief, Y. Z., & Ab. Aziz, N. (2016). Evaluation of solar energy potential in Malaysia. Trends in Bioinformatics, 9(2), 35–43. DOI: https://doi.org/10.3923/tb.2016.35.43
2. Statistics, E. (2019). Handbook Malaysia Energy Statistics. https://meih.st.gov.my/documents/10620/bcce78a2-5d54-49ae-bodc-549dcacf93ae
3. Choi, D. H., Lee, J., Hong, H., & Kang, Y. T. (2014). Thermal conductivity and heat transfer performance enhancement of phase change materials (PCM) containing carbon additives for heat storage application. International Journal of Refrigeration, 42, 112–120. DOI: https://doi.org/10.1016/j.ijrefrig.2014.02.004
4. Kim, S., Jeong, H., Park, J. Y., Baek, S. Y., Lee, A., & Choi, S. H. (2019). Innovative flat-plate solar collector (FPC) with coloured water flowing through a transparent tube. RSC advances, 9(42), 24192–24202. https://doi.org/10.1039/c9ra03442k
5. Nithyanandam, K., & Pitchumani, R. (2014). Optimization of an encapsulated phase change material thermal energy storage system. Solar Energy, 107, 770–788. DOI: https://doi.org/10.1016/j.solener.2014.06.011
6. Barreneche, C., Solé, A., Miró, L., Martorell, I., Fernández, A. I., & Cabeza, L. F. (2013). Study on differential scanning calorimetry analysis with two operation modes and organic and inorganic phase change material (PCM). Thermochimica Acta, 553, 23–26. DOI: https://doi.org/10.1016/j.tca.2012.11.027
7. Sandali, M., Boubekri, A., Benhamza, A., Settou, B., Halassa, D., & Mennouche, D. (2017). A simulation study of a solar collector using phase change materials for air heating application needs. AIP Conference Proceedings, 1814. DOI: https://doi.org/10.1063/1.4976229
8. Khan, M. M. A., Ibrahim, N. I., Mahbubul, I. M., Muhammad. Ali, H., Saidur, R., & Al-Sulaiman, F. A. (2018). Evaluation of solar collector designs with integrated latent heat thermal energy storage: A review. Solar Energy, 166(March 2017), 334–350. DOI: https://doi.org/10.1016/j.solener.2018.03.014
9. Mehrali, M., Latibari, S. T., Mehrali, M., Metselaar, H. S. C., & Silakhori, M. (2013). Shape-stabilized phase change materials with high thermal conductivity based on paraffin/graphene oxide composite. Energy Conversion and Management, 67, 275–282, DOI: https://doi.org/10.1016/j.enconman.2012.11.023
10. Shi, J. N., Ger, M. Der, Liu, Y. M., Fan, Y. C., Wen, N. T., Lin, C. K., & Pu, N. W. (2013). Improving the thermal conductivity and shape-stabilization of phase change materials using nanographite additives. Carbon, 51(1), 365–372. DOI: https://doi.org/10.1016/j.carbon.2012.08.068
11. Huang, Z., Gao, X., Xu, T., Fang, Y., & Zhang, Z. (2014). Thermal property measurement and heat storage analysis of LiNO3/KCl - expanded graphite composite phase change material. Applied Energy, 115, 265–271. DOI: https://doi.org/10.1016/j.apenergy.2013.11.019
12. Cheng, X., Li, G., Yu, G., Li, Y., & Han, J. (2017). Effect of expanded graphite and carbon nanotubes on the thermal performance of stearic acid phase change materials. Journal of Materials Science, 52(20), 12370–12379. DOI: https://doi.org/10.1007/s10853-017-1350-9

13. Du, R., Li, W., Xiong, T., Yang, X., Wang, Y., & Shah, K. W. (2019). Numerical investigation on the melting of nanoparticle-enhanced PCM in latent heat energy storage unit with spiral coil heat exchanger. Building Simulation. 869–879. DOI: https://doi.org/10.1007/s12273-019-0527-3
14. Anusha, G., & Kishore, P. S. (2017). Heat Transfer Analysis of Gasketed Plate Heat Exchanger. October, 8–13. DOI: https://doi.org/10.17950/ijer/v5s12/1215
15. Lin, S. C., Al-Kayuem, H. H., & Aris, M. S. Bin. (2012). Experimental Investigation on the Performance enhancement of Integrated PCM-Flat Plate Solar Collector. DOI: https://doi.org/10.3929/jas.2012.2390.2396
16. Nithyanandam, K., Pitchumani, R., & Mathur, A. (2014). Analysis of a latent thermocline storage system with encapsulated phase change materials for concentrating solar power. Applied Energy, 113, 1446–1460. DOI: https://doi.org/10.1016/j.apenergy.2013.08.053
17. Thirugnanam.C, M. . (2013). Experimental Analysis of Latent Heat Thermal Energy Storage using Paraffin Wax as Phase Change Material. International Journal of Engineering and Innovative Technology (IJEIT), 3(2), 372–376.
18. Bellan, S., Gonzalez-Aguilar, J., Romero, M., Rahman, M. M., Goswami, D. Y., Stefanakos, E. K., & Couling, D. (2014). Numerical analysis of charging and discharging performance of a thermal energy storage system with encapsulated phase change material. Applied Thermal Engineering, 71(1), 481–500. DOI: https://doi.org/10.1016/j.applthermaleng.2014.07.009
19. El Qarnia, H. (2009). Numerical analysis of a coupled solar collector latent heat storage unit using various phase change materials for heating the water. Energy Conversion and Management, 50(2), 247–254. DOI: https://doi.org/10.1016/j.enconman.2008.09.038
20. Alva S, L. H., González, J. E., & Dukhan, N. (2006). Initial analysis of PCM integrated solar collectors. Journal of Solar Energy Engineering, Transactions of the ASME, 128(2), 173–177. DOI: https://doi.org/10.1115/1.2188532
21. Fang, G., Li, H., Yang, F., Liu, X., & Wu, S. (2009). Preparation and characterization of nano-encapsulated n-tetradecane as phase change material for thermal energy storage. Chemical Engineering Journal, 153(1–3), 217–221. DOI: https://doi.org/10.1016/j.cej.2009.06.019
22. Ren, W., Cao, L., & Zhang, D. (2020). Composite phase change material based on reduced graphene oxide/expanded graphite aerogel with improved thermal properties and shape-stability. International Journal of Energy Research, 44(1), 242–256. DOI: https://doi.org/10.1002/er.4900
23. Jin, Y., Wan, Q., & Ding, Y. (2015). PCMs heat transfer performance enhancement with expanded graphite and its thermal stability. Procedia Engineering, 102, 1877–1884. DOI: https://doi.org/10.1016/j.proeng.2015.01.326
24. Li, M., Chen, M., Wu, Z., & Liu, J. (2014). Carbon nanotube grafted with polyalcohol and its influence on the thermal conductivity of phase change material. Energy Conversion and Management, 83, 325–329. DOI: https://doi.org/10.1016/j.enconman.2014.04.002
25. Luu, M. T., Milani, D., Nomvar, M., & Abbas, A. (2020). A design protocol for enhanced discharge exergy in phase change material heat battery. Applied Energy, 265(February), 114801. DOI: https://doi.org/10.1016/j.apenergy.2020.114801
26. Duraković, B. (2020). PCM-Based Building Envelope Systems - Innovative Energy Solutions for Passive Design. DOI: https://doi.org/10.1007/978-3-030-38335-0
27. Elmozughi, A. F., Solomon, L., Oztekin, A., & Neti, S. (2014). Encapsulated phase change material for high temperature thermal energy storage - Heat transfer analysis. International Journal of Heat and Mass Transfer, 78, 1135–1144. DOI: https://doi.org/10.1016/j.proeng.2015.01.326